Catalysis Science & Technology

ROYAL SOCIETY OF CHEMISTRY

PAPER

View Article Online
View Journal | View Issue

Cite this: *Catal. Sci. Technol.*, 2026, **16**, 2522

Tangled effects of CuCl precursor and Zn and Sn promoters used for the direct synthesis of methylchlorosilanes

L. Riviere,[a] E. Blaser,[b] M. Huet,[b] C. Rosier,[b] C. Geantet[a] and S. Loridant *[a]

Received 26th November 2025,
Accepted 21st February 2026

DOI: 10.1039/d5cy01426c

rsc.li/catalysis

In this work, the effects of CuCl precursor and Zn and Sn additives on the formation of Cu-based metallic phases as well as on catalytic performance and coke formation were investigated during the early stage of methylchlorosilane synthesis. The Cu_3Si catalytic active phase, as well as $Cu_{15}Si_4$ and Cu, is formed during pretreatment at 310 °C. Addition of Zn and $Cu_{0.9}Sn_{0.1}$ was shown to accelerate their formation probably through the wetting of Si particles by mixed chlorides. Furthermore, residual chloride particles were observed both for promoted and unpromoted masses. It was confirmed that Zn and Sn promote the dimethyldichlorosilane formation rate at 295 °C but also clearly showed that they favour CH_3Cl cracking. Coke containing disordered graphite, readily detected by Raman spectroscopy, was preferentially formed on residual chloride particles. CH_3Cl cracking could be favoured by the presence of Zn and Sn within such particles. Therefore, the tangled positive and negative effects of Zn and Sn 'promoters' as well as of the CuCl precursor highlight the need to carefully optimize their respective amounts in an industrial process.

1. Introduction

The Müller–Rochow process (also called direct synthesis) involves the reaction of methyl chloride with silicon to produce methylchlorosilanes (MCSs) in the presence of a copper-based catalyst. The main reaction leads to the formation of dimethyldichlorosilane (labelled M2) as follows:

$$Si(s) + 2\ CH_3Cl(s) \rightarrow (CH_3)_2SiCl_2(g) \quad (1)$$

M2 is used industrially as a precursor for silicone production, representing a global market valued at approximately 10 billion USD and an annual production capacity of 2.1 million tons.[1]

The Müller–Rochow process is performed industrially in a continuous fluidized bed reactor in which Si particles are mixed with a copper-based catalyst and Zn and Sn-based promoters to form the contact mass. A continuous flow of CH_3Cl gas passes through the bed to fluidize the solid particles. This fluidization enables efficient heat transfer and generally allows better control of the temperature and prevents hot spots that could lead to CH_3Cl thermal cracking.[2]

Recently, an overview of the advances in the Müller–Rochow process has been reported.[3] This provides a critical assessment of the direct synthesis from both chemical and sustainability perspectives. It highlights the need to establish clear structure–activity relationships and to better control product selectivity. Moreover, the reaction mechanism, which is still not fully understood, could be resolved with advanced *in situ* and *operando* characterization techniques combined with DFT and kinetic modelling. Finally, sustainability issues, such as catalyst recycling or silicone residue reuse are identified as equally critical for achieving a more efficient and economically sustainable silicone industry.

From a catalytic point of view, several Cu-based precursors can be used in the Müller–Rochow reaction. When Cu or CuO are used as catalyst precursors, they must first be chlorinated by reaction with CH_3Cl to form CuCl resulting in an induction period. To shorten this period, CuCl is often used directly as the copper precursor.[4–6] Above 200 °C, CuCl can be reduced either to Cu_3Si, active in M2 synthesis, or to Cu, which promotes the CH_3Cl cracking.[7] Other Cu–Si intermetallic phases such as Cu_5Si and $Cu_{15}Si_4$ are present during the reaction and may exhibit a catalytic activity in M2 synthesis.[5,8] However, the use of these Cu-rich compounds leads to a rapid loss of selectivity due to their transformation into Cu through Si consumption[9] and their reaction with CuCl to form Cu.[10]

To improve selectivity toward M2, copper oxide precursors promoted with different additives have been investigated. Recent studies have shown that the Cu_2O or CuO precursor can benefit from Zn, Sn and P-based promoters.[11–13] These additives enhance Cu^+ reduction, increase surface oxygen

[a] *Université Claude Bernard Lyon 1, CNRS, IRCELYON, UMR 5256, Villeurbanne, F-69100, France. E-mail: stephane.loridant@ircelyon.univ-lyon1.fr*
[b] *R&D Laboratory, Elkem Silicones France, 69190 Saint Fons, France*

species and strengthen electronic interactions, thereby facilitating the formation of the Cu_3Si active phase and improving both activity and M2 selectivity. However, the Cu and CuCl phases are inactive in MCS synthesis but active in CH_3Cl cracking, producing liquid and solid hydrocarbons (coke).[7] Such deposits disturb reactor operation and deteriorate performance by covering active sites, causing catalyst deactivation.[14,15] Other by-products from this side reaction include low-boiling hydrocarbons (CH_4, C_2H_6, C_3H_8,…) as well as HCl and Cl_2. They can further react to form hydrogenated chlorosilanes such as CH_3HSiCl_2, thereby reducing selectivity toward M2 in the direct synthesis.[16]

Zinc and tin promoters are widely used to enhance both the reaction rate and M2 selectivity in the direct synthesis.[4,15–22] Recently, Su and co-workers have reported several studies[23–25] on the role of Zn-based promoters in the phase transformation of copper oxide precursors during the Müller–Rochow reaction. The introduction of Zn, ZnO or mixtures of ZnO, Sn and P enhance CH_3Cl adsorption on CuO or Cu_2O surfaces, thereby accelerating their transformation into CuCl and Cu and promoting the formation of the Cu_3Si active phase. Notably, the ZnO–Sn–P system[25] enables the direct conversion of CuO into the CuCl and Cu phases without a Cu_2O intermediate. In another study,[26] the same group showed that adding SnO_2 to the Cu_2O precursor also accelerates phase transformation, leading to improved catalytic performance.

However, few studies have investigated the effect of promoters in relation to coke formation during MCS synthesis. For instance, one study reported that zinc facilitates the conversion of silicon carbide into graphite,[21] while another work showed that increasing the proportion of $ZnCl_2$ in a contact mass promotes CH_4 formation, indicating enhanced CH_3Cl cracking.[16] Gasper-Galvin *et al.* proposed that Zn and Sn promoters improve copper dispersion on the silicon surface.[22] This hypothesis was supported by Wessel and Rethwisch, whose Auger analysis revealed that the Cu/Si ratio in a Si/Cu/Zn/Sn contact mass was more than twice that observed for Cu_3Si samples.[15] Consequently, in promoted contact masses (Si/Cu/Zn/Sn), copper predominantly exists as a finely dispersed copper silicide phase, whereas unpromoted samples (Si/Cu) exhibit lower copper dispersion and a higher fraction of bulk metallic copper. The increased concentration of metallic Cu sites was correlated with the higher coking rates observed in their experiments. Similarly, another study suggests that Zn promotes copper dispersion and facilitates the formation of the active phase.[27] Their results also indicate that Zn promotes the structural order (graphitization) of deposited coke and reduces its hydrogen content, consistent with the findings of Frank *et al.*[21]

In the present work, the effect of Zn ($ZnCl_2$) and $Cu_{0.9}Sn_{0.1}$ addition on both the formation of Cu-based metallic phases from the CuCl precursor as well as on either catalytic performance and coke formation was investigated during the early stage of MCS synthesis, revealing tangled effects. To this end, promoted and unpromoted contact masses with varying promoter loadings were evaluated in a batch reactor and characterized using XRD, SEM-EDS, TPO and Raman techniques.

2. Experimental methods

2.1 Contact masses

Silicon powder (50–80 μm) was obtained from Elkem company. CuCl, Zn and $Cu_{0.9}Sn_{0.1}$ bronze used to prepare contact masses were purchased from commercial suppliers. CuCl (<125 μm) was obtained from Merck Sigma-Aldrich (reference 1027390250). Zn (<160 μm) and $Cu_{0.9}Sn_{0.1}$ bronze (<160 μm) was obtained from Elkem company. The four different contact masses used for this study are presented in Table 1. Non-promoted mass (labelled NPM) contains only Si (96.60 wt%) and CuCl (3.40 wt%) while tin was added as the $Cu_{0.9}Sn_{0.1}$ precursor to all promoted masses and zinc was added either directly (PM-Zn0.05 and PM-Zn0.30 containing 0.05 and 0.30 wt% of Zn, respectively) or as $ZnCl_2$ (PM-$ZnCl_2$-Zn0.30). The Si mass was adjusted to obtain the Cu, Zn, and Sn contents reported in Table 1, leading to Si contents being quite similar (from 96.28 to 96.60 wt%). The copper precursor and Zn and Sn-based promoters used here are representative of the one employed in industry.

2.2 Catalytic testing

60 g of contact mass was loaded in a stirred batch reactor of 300 mL (scheme in Fig. S1), which was purged three times with 3 bar of Ar. For pretreatment, the reactor was pressurized with 1 bar of Ar and the temperature was increased from room temperature (RT) until either 200 °C or 310 °C at a rate of 10 °C min^{-1}. The temperature was maintained constant for approximately two hours before depressurisation to ambient pressure and cooling to 200 °C.

For catalytic testing, the reactor was purged three times with 3 bar of CH_3Cl before depressurisation to 1 bar. The temperature was then increased from 200 to 280 °C for 10 min with a heating rate of 8 °C min^{-1}. Finally, a slower rate of 1 °C min^{-1} was applied for 15 min until 295 °C to limit exothermicity. A stirring velocity was maintained at 150 rpm during the pretreatment and the reaction. The temperature and pressure ranges used industrially for the direct synthesis (typically 260–310 °C and 2–7 bar) are comparable to those employed in the present study.

Once the reaction was completed, the temperature was stopped, and the pressure was released to condense MCS products and collect incondensable gases. For that purpose, the outlet line, heated at 110 °C, was connected to a MCS trap cooled by a cryostat at −12 °C, which enabled to condense all major MCS products ($(CH_3)_2SiCl_2$ (M2), $(CH_3)SiCl_3$ (M1), $(CH_3)_3SiCl$ (M3), $(CH_3)HSiCl_2$ (MH), $SiCl_4$ and $(CH_3)_2Si_2Cl_4$) and analysed them offline using a Shimadzu GC-2014 chromatograph equipped with one PERMABOND Silane capillary GC column (50 m × 0.32 mm). A cylinder of 5

Table 1 Weight compositions of the prepared contact masses

Contact mass	Labelling	Cu content (wt%)	Zn content (wt%)	Sn content (wt%)
Si/CuCl	NPM	3.40	—	—
Si/CuCl/Zn/$Cu_{0.9}Sn_{0.1}$	PM-Zn0.05	3.40	0.05	0.02
Si/CuCl/Zn/$Cu_{0.9}Sn_{0.1}$	PM-Zn0.30	3.40	0.30	0.02
Si/CuCl/$ZnCl_2$/$Cu_{0.9}Sn_{0.1}$	PM-$ZnCl_2$-Zn0.30	3.40	0.30	0.02

L was linked to the cryostat output in order to collect non-condensed gases (N_2, CH_3Cl, H_2, CH_4, C_2H_6 and C_2H_4) and unreacted CH_3Cl before analysis by online analysis using a Shimadzu GC-2014 chromatograph equipped with one Carboxen 1010 PLOT capillary GC column (30 m × 0.32 mm). N_2 was used as the internal standard adding a flow of 2.5 mL min^{-1} to the flow of 9.3 mL min^{-1} coming from the cylinder. The data collected during calibration and catalytic testing were processed with the Lab-Solutions software.

The X_{CH_3Cl} conversion is provided by eqn (2):

$$X_{CH_3Cl}\,(\%) = \frac{n(CH_3Cl)_{in} - n(CH_3Cl)_{out}}{n(CH_3Cl)_{in}} \times 100 \quad (2)$$

where $n(CH_3Cl)_{in}$ and $n(CH_3Cl)_{out}$ correspond to the number of moles of CH_3Cl reagent introduced into the reactor and at the outlet of the reactor, respectively.

The X(Si) conversion was calculated from the Si atom balance over all MCS products analysed at the reactor outlet. It is provided by eqn (3):

$$X(\mathrm{Si})\,(\%) = \frac{n(\mathrm{M1})_{out} + n(\mathrm{M2})_{out} + n(\mathrm{M3})_{out} + n(\mathrm{MH})_{out} + n(\mathrm{SiCl_4})_{out} + 2n\left((\mathrm{CH_3})_2\mathrm{Si_2Cl_4}\right)_{out}}{n(\mathrm{Si})_{in}} \times 100 \quad (3)$$

where $n(Si)_{in}$ corresponds to the number of moles of Si reagent introduced into the reactor and $n(MCS)_{out}$ corresponds to the number of Si moles of a MCS product at the outlet of the reactor.

The initial reaction rate r is defined according to the eqn (4):

$$r\left(g_{CH_3Cl}\,kg_{Si}^{-1}\,h^{-1}\right) = \frac{m(CH_3Cl)_{out} - m(CH_3Cl)_{in}}{m(Si)_{in} \times t} \quad (4)$$

where $m(CH_3Cl)_{in}$ and $m(CH_3Cl)_{out}$ corresponds to the weight (expressed in g) of CH_3Cl reagent introduced into the reactor and at the outlet of the reactor, respectively, $m(Si)_{in}$ corresponds to the weight (expressed in kg) of Si introduced into the reactor, and t corresponds to 15 min of reaction protocol.

The silicon selectivity to a MCS product is defined by the ratio of the number of Si moles of this product to the total number of Si moles of analysed MCS products. For instance, the selectivity to M2, S(M2) is given by eqn (5):

$$S(\mathrm{M2})\,(\%) = \frac{n(\mathrm{M2})_{out}}{n(\mathrm{M1})_{out} + n(\mathrm{M2})_{out} + n(\mathrm{M3})_{out} + n(\mathrm{MH})_{out} + n(\mathrm{SiCl_4})_{out} + 2n((\mathrm{CH_3})2\,\mathrm{Si_2Cl_4})_{out}} \times 100 \quad (5)$$

The carbon yield of CH_4, Y_{CH_4}, which is an indicator of CH_3Cl cracking, was calculated with eqn (6):

$$Y_{CH_4}\,(\%) = \frac{n(CH_4)_{out}}{n(CH_3Cl)_{in}} \times 100 \quad (6)$$

where $n(CH_4)_{out}$ corresponds to the number of CH_4 moles at the outlet of the reactor. The amounts of H_2, C_2H_6 and C_2H_4 produced were quite low (<0.1%).

The yield of carbon deposited on the mass was determined through TPO analysis considering total oxidation during TPO measurement ($C + O_2 \rightarrow CO_2$). The use of a mass spectrometer was allowed to quantify low carbon content (<0.1%).

Catalytic testing has been performed in a batch reactor at different transformation rates of Si (less than 14%) and at different conversions of CH_3Cl ($20\% < X(CH_3Cl) < 90\%$) in order to investigate the initiation of CH_3Cl cracking during the MCS synthesis. The $Y(CH_4)$ yield, the C content and MCS selectivity values were correlated with the quantity of Cu and Cu_3Si crystalline phases characterized by XRD diffraction. Therefore, although the present experiments are performed at low Si conversion, they are specifically designed to investigate reaction conditions that are highly representative of those encountered in industrial reactors, particularly regarding the onset of CH_3Cl cracking.

2.3 Characterization tools

X-ray diffraction (XRD) analysis was carried out with a Brucker D8 Advance 25 diffractometer. The X-ray source, used with a power of 1.75 kW, was composed of a tungsten cathode and a copper anode. A Ni filter almost completely vanished the Cu K_β line. The diffractograms were recorded from 42° to 46° (2θ) with a step of 0.02° and 4 s of counting per point. The divergence slit was fixed at 1.0° instead of 0.2° usually used in order to improve the counting rate. The size of the divergence slit influences the peak intensities and shapes. A rotation of the sample was done at 15 rpm so as to avoid preferential orientations. Cu_3Si being extremely air sensitive, an inerting method was used.

Scanning electron microscopy (SEM) images were collected with a FEI/Philips XL-30 Field Emission ESEM microscope under a high vacuum of $\times 10^{-6}$ Pa, the beam energy was varied from 10 to 20 keV and the magnification from ×100 to ×5000. Localized chemical analysis was performed with energy dispersive X-ray spectroscopy (EDS), utilizing the K_α X-ray lines of the elements. No preparation of the contact masses was necessary due to their conductive nature.

The sample was grinded under Ar before temperature programmed oxidation (TPO) analysis in order to minimize the influence of non-uniform distribution of coke in the mass due to its really low content (less than 1%). 360 mg of the sample was used in order to maximize the representativeness of the 60 g of mass used during direct synthesis. The sample was heated under a flowing gas mixture (45 mL min^{-1}) of 1% O_2 in He at a rate of 7 °C min^{-1} up to 600 °C and was kept as this temperature for 20 min before cooling down to room temperature. Analysis of CO and CO_2 products was performed by mass spectrometry. CO was produced in a negligible amount therefore is no longer discussed in this paper.

Raman spectra were recorded with a LabRam HR Evolution (Jobin Yvon-Horiba) spectrometer. Mappings were performed due to the heterogeneity of masses and in order to detect if traces of disordered graphite (a part of coke) were formed at the beginning of the CH_3Cl cracking. An exciting line at 532 nm of solid-state laser was used. The power at the sample was around 1 mW. A microscope objective with a magnification of ×50 was used to focus the incident beam and recollect the scattered light which was spatially dispersed with a 300 lines per mm diffraction grating leading to a spectral resolution of 4 cm^{-1}. The spatial resolution was about 2 microns. The mapping area was 100 per 100 μm^2 with a step of 4 μm along the x and y axes (676 spectra). The acquisition time was 50 s for each spectrum. As the used masses were photoluminescent leading to significant background, it was previously subtracted. Correlative microscopy was carried out using a Nano-GPS system, which enabled rapid and precise relocation of points of interest between Raman and SEM analyses.

3. Results and discussion

3.1 Effects of Zn and Sn promoters on thermal activation

A thermal pre-treatment at 310 °C under 1 bar of Ar was performed in the batch reactor prior to catalytic testing in order to already form the Cu_3Si active phase and hence temporally separate the activation and reaction steps. Fig. S2 displays the temporal evolution of reactor temperature and pressure for the PM-Zn0.30 promoted contact mass. A first increase in pressure is observed due to the rise in temperature with a slight delay probably due to the thermal inertia of the batch reactor. After stabilization, the pressure suddenly re-increases up to *ca.* 4 bar. It was related to the formation of gaseous $SiCl_4$ as revealed by mass spectrometry and could be associated with formation of Cu_3Si according to chemical eqn (7):

$$12\ CuCl(s) + 7\ Si(s) \rightleftarrows 4\ Cu_3Si(s) + 3\ SiCl_4(g) \quad (7)$$

However, the formation of other metallic Cu compounds such as Cu, Cu_5Si and $Cu_{15}Si_4$ (denoted as $Cu_{3.75}Si$) also leads to the formation of $SiCl_4$ in the same proportion (1 mole for 4 moles of CuCl):

$$4\ CuCl(s) + Si(s) \rightleftarrows 4\ Cu(s) + SiCl_4(g) \quad (8)$$

$$20\ CuCl(s) + 9\ Si(s) \rightleftarrows 4\ Cu_5Si(s) + 5\ SiCl_4(g) \quad (9)$$

$$15\ CuCl(s) + 7.75\ Si(s) \rightleftarrows 4\ Cu_{3.75}Si(s) + 3.75\ SiCl_4(g) \quad (10)$$

The calculated free Gibbs energies at 310 °C (583 K) were −235, −192, −371 and −280 kJ mol^{-1} (see thermodynamic calculations in the SI and Tables S1 and S2), respectively, showing that the four reactions are thermodynamically favourable and hence they could contribute to the pressure rise. By performing the experiment three times, the average onset time of pressure rise corresponding to the $SiCl_4$ release was *ca.* 60 min with a relative standard deviation of 14%.

XRD analysis was used to identify the crystalline phases and determine the reactions involved in the contact mass. The diffractogram of PM-Zn0.30 pre-treated at only 200 °C (Fig. 1a) did not reveal the presence of copper silicides while the $Cu_{15}Si_4$ and Cu_3Si crystalline phases and to a lesser extent Cu were present after pre-treatment at 310 °C (Fig. 1b).

The peak at 43.67° could be attributed to Cu_5Si but its second main peak should appear near 46.1° which is not the case (the small peak systematically observed is due to Si).[28] Concerning the peaks at 44.56 and 45.14°, the best match was obtained with the PDF 076-7859 pattern which corresponds to one $Cu_{3.17}Si$ phase.

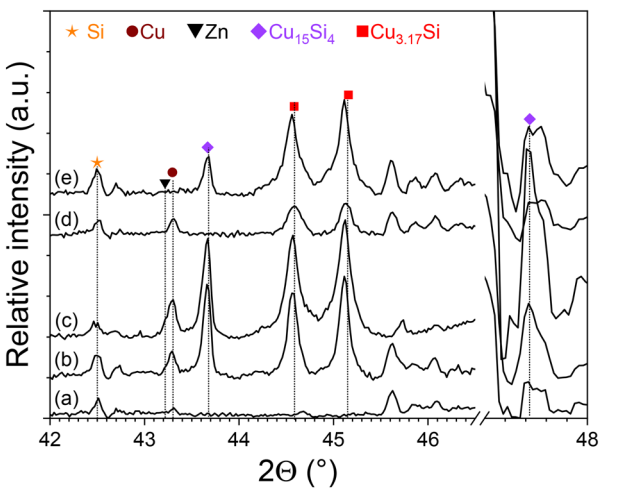

Fig. 1 XRD diffractograms in the 2θ angle range of 42–46° of (a) PM-Zn0.30 contact mass pre-treated at 200 °C (b) PM-Zn0.30 pre-treated at 310 °C, (c) PM-$ZnCl_2$-Zn0.30, (d) PM-Zn0.05 and e) NPM. The symbols indicate the peak positions of the Si, Cu, Zn, $Cu_{15}Si_4$, $Cu_{3.17}Si$ crystalline phases, which were indexed with the PDF 27-1402, 04-0836, 04-0831, 14-4307 and 76-7859 patterns, respectively.

Six distinct phases, labelled η‴, η″, η′, η_3, η_2, η_1 were identified when increasing temperature.[29] The η‴ phase was stable under ambient conditions and up to 285 ± 15 °C for $Cu_{74}Si_{26}$ and 315 ± 15 °C for $Cu_{78}Si_{22}$ whereas the η″ phase was stable from 285–315 to 375–475 °C. The two phases can be indexed using a similar trigonal unit cell, but they differ in their superstructures or modulation vectors.[29] As XRD analysis was performed at ambient temperature, the peaks at 44.56 and 45.14° were attributed to the η‴ phase while an interplay between the η‴ and η″ phases could occur both during pre-treatment at 310 °C and reaction at 295 °C. Note that the Cu/Si ratio of the η″ Cu_3Si phase ranges from 3.0 to 3.2–3.3 in the reported Cu–Si phase diagrams.[30–32]

Considering the XRD results, the $SiCl_4$ release leading to the second pressure rise is associated with formation of the Cu, $Cu_{15}Si_4$ and Cu_3Si phases, which appear to be simultaneous. The quantity of $SiCl_4$ calculated considering complete consumption of CuCl was 0.0076 moles. This corresponds to a variation of pressure of 1.2 bar which is *ca.* 30% higher than the measured values. This suggests that CuCl consumption is not complete when stopping thermal pre-treatment and residual CuCl should be present in the masses.

Interestingly, the onset time of pressure rise is lowered by adding Zn and $Cu_{0.9}Sn_{0.1}$ powders to the contact mass (Table 2), largely exceeding the uncertainty derived from repeatability. The onset time is even smaller when Zn is directly added as $ZnCl_2$ powder (40 min for PM-$ZnCl_2$-Zn0.30 instead of 60 min for PM-Zn0.30).

The formation of Cu_3Si at 310 °C was evidenced by XRD (Fig. 1) for both the promoted and non-promoted masses while a relatively high amount of $Cu_{15}Si_4$ and to a lesser extent Cu was present in PM-Zn0.30 and PM-$ZnCl_2$-Zn0.30 (Fig. 1b and c, respectively). In contrast, only a small quantity of either Cu or $Cu_{15}Si_4$ was detected for PM-Zn0.05 and NPM (Fig. 1d and e, respectively). The presence of Cu does not arise from dealloying of $Cu_{0.9}Sn_{0.1}$ bronze since this phase is stable during thermal treatment at 310 °C (Fig. S3).

Even if the formation of Cu, Cu_3Si and $Cu_{15}Si_4$ by the reaction of CuCl with Si is highly favourable, kinetics should be slow because of solid–solid reactions. Considering the CuCl–$ZnCl_2$ phase diagram containing an eutectic with a fusion temperature at 230–240 °C,[33] a part of the CuCl–$ZnCl_2$ mixture is liquid at 310 °C favouring the wetting of Si particles, thereby accelerating the formation of Cu-based phases including Cu_3Si. When adding Zn, the formation of $ZnCl_2$ can occur during pretreatment according to eqn (11), which is thermodynamically favourable ($\Delta G°(310\ °C) = -132$ kJ mol^{-1}):

$$2\ CuCl(s) + Zn(s) \rightleftarrows 2\ Cu(s) + ZnCl_2(s) \quad (11)$$

As the CuCl–$SnCl_2$ mixture also exists in both the liquid and solid phases at 310 °C, a similar accelerating effect is expected when adding $SnCl_2$ directly. When adding $Cu_{0.9}Sn_{0.1}$, $SnCl_2$ has to be previously formed according to eqn (12):

$$0.2\ CuCl(s) + Cu_{0.9}Sn_{0.1}(s) \rightleftarrows 1.1\ Cu(s) + 0.1\ SnCl_2(s) \quad (12)$$

However, this reaction leads to the formation of a small quantity of $SnCl_2$ (compared to $ZnCl_2$ for PM-Zn0.30) and is poorly favourable ($\Delta G°(310\ °C) = -32$ kJ mol^{-1}). Therefore, its contribution should be negligible.

Finally, considering the ternary CuCl–$ZnCl_2$–$SnCl_2$ phase diagram, a large range of compositions was found to give melt formation below 310 °C.[34] Therefore, the presence of both $ZnCl_2$ and $SnCl_2$ strongly facilitates the formation of not only Cu_3Si but also of the unselective Cu and $Cu_{15}Si_4$ phases.

The activated masses were further characterized using SEM and EDS techniques. Both compact particles of *ca.* 100 μm and small agglomerates were observed in the SEM images of NPM (Fig. 2a).

Cl and Cu were detected in the areas corresponding to agglomerates confirming that CuCl did not totally react during pre-treatment. EDS analysis also revealed the Cu migration onto Si particles, which is necessary to form Cu_3Si.[35] Such phenomenon was also observed for the PM-Zn0.30 contact mass pretreated at 310 °C (Fig. 2c) but not at 200 °C (Fig. 2b). Furthermore, Cl was detected in the same locations as Cu and Zn, supporting the hypothesis of mixed chloride formation during pre-treatment. However, the large (*ca.* 100 μm) agglomerate observed in the SEM image does not look like a molten salt. Note that Sn was not detected, probably due to its low amount and that the mixed chloride could contain Sn.

3.2 Early stages of the MCS synthesis

Catalytic testing has then been performed in a batch reactor at very low Si conversion (0.5–0.6%) using the pretreated masses listed in Table 1 in order to investigate the effect of adding Zn and $Cu_{0.9}Sn_{0.1}$ on the performance of the MCS synthesis.

Table 2 Onset times of ΔP pressure rise for different masses with or without Zn and $Cu_{0.9}Sn_{0.1}$ addition

Contact mass	Onset time of ΔP (min)
NPM	250
PM-Zn0.05	110
PM- Zn0.30	60
PM-$ZnCl_2$-Zn0.30	40

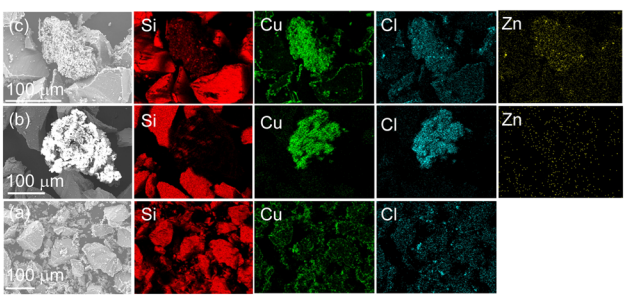

Fig. 2 SEM images and the corresponding EDS elemental mapping images of (a) NPM pretreated at 310 °C, and PM-Zn0.30 pretreated (b) at 200 °C and (c) at 310 °C.

As shown in Table S3, the CH_3Cl conversion was almost complete after 30 min at 295 °C using pre-treated PM-Zn0.30 and M2 was produced selectively (75%). Catalytic performance obtained for three tests were repeatable (standard deviations below 2%). The pressure drop observed over time (Fig. S4) is mostly due to the M2 formation by CH_3Cl (and Si) consumption. Note that the relative pressure started to decrease at only 246 °C (after 5 min of reaction protocol during temperature rise) revealing that the catalyst is activated before the end of the temperature rise. The evolutions of temperature and pressure were quite repeatable.

It was previously reported that the reaction rate at 300 °C increased from 9.6 g_{CH_3Cl} kg_{Si}^{-1} h^{-1} for an unpromoted Si/CuCl mass to 29 g_{CH_3Cl} kg_{Si}^{-1} h^{-1} for a Si/CuCl/$ZnCl_2$ (Zn = 0.5 wt%) mass and to 40 g_{CH_3Cl} kg_{Si}^{-1} h^{-1} for a Si/CuCl/$ZnCl_2$/$SnCl_2$ (Zn = 0.5 wt%, Sn = 0.01 wt%) mass.[18] Likewise, the steady-state rate of M2 production at 290 °C for the Si/Cu/Zn/Sn (1 wt% Zn, 0.02 wt% Sn) mass was more than 50 times greater than that for the Si/Cu mass.[15] In the present study, it was found that the addition of Zn and Sn at only 0.05 and 0.02 wt% (PM-Zn0.05), respectively, allows to slightly increase the initial reaction rate at 295 °C from 27 to 35 g_{CH_3Cl} kg_{Si}^{-1} h^{-1}. It reached 62 g_{CH_3Cl} kg_{Si}^{-1} h^{-1} at 0.30 wt% of Zn (PM-Zn0.30), while using $ZnCl_2$ instead of Zn as a precursor (PM-$ZnCl_2$-Zn0.30) further promotes the initial rate to 76 g_{CH_3Cl} kg_{Si}^{-1} h^{-1}.

The addition of Zn and $Cu_{0.9}Sn_{0.1}$ to the NPM contact mass was confirmed to increase the M2 selectivity in agreement with previous studies (Fig. S5a).[15,18] However, higher CH_4 yields were obtained at high CH_3Cl conversion for the promoted masses (Fig. S5b) indicating more cracking reactions. This result is consistent with the higher quantity of the Cu and $Cu_{15}Si_4$ crystalline phases in these masses after pre-treatment (Fig. 1) while the quantity of Cu_3Si is equivalent. Indeed, the $Cu_{15}Si_4$ phase can lead to Cu (by Si consumption), which is known to catalyse the CH_3Cl cracking, and causing rapid deactivation of the mass at higher Si conversion.[7,8,10] Consistently, the TPO-MS curves of the different masses after reaction (Fig. S6) reveal that less carbon is deposited on the NPM and the PM-Zn0.05 contact masses, with only 10–15 ppm of carbon detected, compared to 35–50 ppm for PM-$ZnCl_2$-Zn0.30 and PM-Zn0.30 masses.

Fig. 3 shows the XRD diffractograms of the four contact masses after 30 min of reaction (*ca.* 90% of CH_3Cl conversion, 0.5–0.6%% of Si conversion). The relative intensity of the Cu peak was much higher than those of the Cu_3Si and $Cu_{15}Si_4$ peaks, revealing important structural evolution during the reaction. It was particularly the case for the NPM contact mass for which the intensity of the Cu_3Si peaks was low. Cu formation could result from the consumption of Si atoms at the surface of the Cu_3Si and $Cu_{15}Si_4$ phases to produce MCS products. However, as the presence of CuCl was still evidenced by SEM/EDX analysis after reaction for unpromoted and promoted masses (Fig. S7), this suggests that the reaction between CuCl and Si leading to Cu and $SiCl_4$ formation according to eqn (8) would accelerate under chlorinated gases by chlorination of the Si surface.[6]

The relative intensities of Cu_3Si and $Cu_{15}Si_4$ peaks were much higher for the two high Zn content masses (PM-Zn0.30 and PM-$ZnCl_2$-Zn0.30) confirming that Zn favours Si diffusion enabling to rapidly reform those copper silicides.[36] Furthermore, the Cu peak was slightly shifted to a lower 2θ angle (especially for PM-$ZnCl_2$-Zn0.30) suggesting the increase in the unit cell parameter by Zn incorporation.[37]

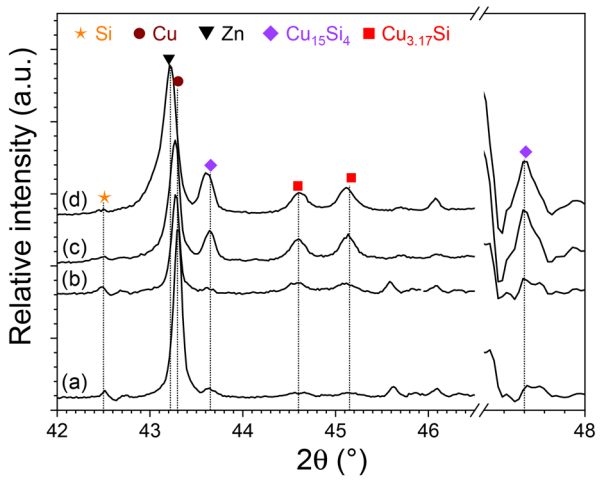

Fig. 3 XRD diffractograms between 42–51° of (a) NPM, (b) PM-Zn0.05, (c) PM-Zn0.30 and (d) PM-$ZnCl_2$-Zn0.30 contact masses after reaction at 295 °C (89–92% of CH_3Cl conversion, 0.5–0.6% of Si conversion). The symbols indicate the peak positions of the Si, Cu, Zn, $Cu_{15}Si_4$, $Cu_{3.17}Si$ crystalline phases, which were indexed with the PDF 27-1402, 04-0836, 04-0831, 14-4307 and 76-7859 patterns, respectively.

3.3 Increasing Si conversion

CH_3Cl cracking occurs at the beginning of the MCS synthesis, leading to the formation of carbonaceous species. However, our reaction conditions (volume of CH_3Cl, mass of Si) led to high CH_3Cl conversions (90%), which prevents the Si conversion increase in one run. Therefore, to reach a

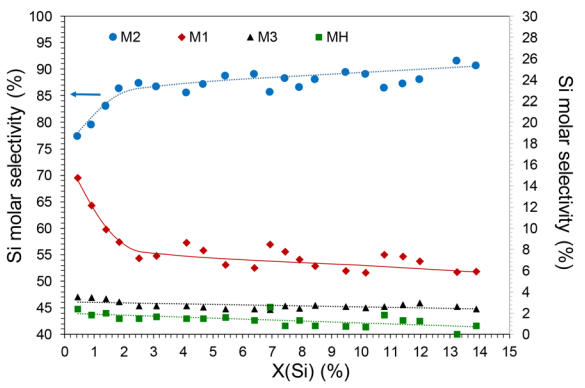

Fig. 4 Evolution the Si molar selectivity of the main MCS products with Si conversion for PM-Zn0.30 pretreated mass.

higher coke content, 24 consecutive injections of CH_3Cl were carried out allowing to reach up to 13.9% of Si conversion with the PM-Zn0.30 pretreated mass. The CH_3Cl conversion remained around 90% after 30 min for each reinjection. Fig. 4 shows the evolution of the Si molar selectivity of the main MCS products. The data reveal that the M2 selectivity value increased to approximately 90%, while the M1 one dropped to 6% and the M3 and MH ones remain constant throughout the reaction. The selectivity values to $SiCl_4$ and $Me_2Si_2Cl_4$ were quite low (<1%).

The samples were collected from the contact mass at Si conversions of 1.5%, 6.4%, 10.2% and 13.9% to examine the evolution of carbon content. The TPO curves indicate that the carbon content increases with Si conversion and reaches 760 ppm at 13.9% of Si conversion (Fig. 5).

Overall, the carbon production increased linearly with the cumulative reaction time as the M2 one (Fig. S8) but with a rate 700 times lower (0.06 g_C kg_{Si}^{-1} h^{-1} *versus* 43.95 g_{M2} kg_{Si}^{-1} h^{-1}).

The XRD diffractograms plotted as shown in Fig. 6 indicate that Cu_3Si peaks remained constant while the $Cu_{15}Si_4$ one increased in spite of the Si consumption due to MCS synthesis. As already mentioned, such (re)-generation of copper silicides by Si diffusion would be favoured by the presence of Zn.[36] Furthermore, the relative intensity of the Cu peak remained high, however, a new component appeared around 43.1°, which may result from Zn diffusion into Cu, forming a Cu–Zn brass alloy.[38]

After the reaction at X(Si) = 1.5%, the PM-Zn0.30 contact mass contained only 80 ppm of C, which was not detected by EDX analysis. Raman mapping of a 100 × 100 μm^2 area of this mass was carried. An optical image of the analysed area (Fig. 7a) shows that it consisted of a mixture of both Si (on the left) and metal chloride (on the right) particles. A fluorescence background superimposed on the Raman signal was systematically observed suggesting the presence of aromatic compounds (Fig. S9). After subtraction of this background, the main band of crystalline Si at 521 cm^{-1} and the second order bands at 300, 615 and 935–990 cm^{-1} were distinguished.[39,40] Furthermore, the presence of disordered graphite (a part of coke) was characterized by the G-band around 1580 cm^{-1}, corresponding to the graphitic lattice mode with the E_{2g} symmetry and the D-band at 1350 cm^{-1}, corresponding to defects present in graphitic plans with the A_{1g} symmetry.[41] Raman spectroscopy is highly sensitive to

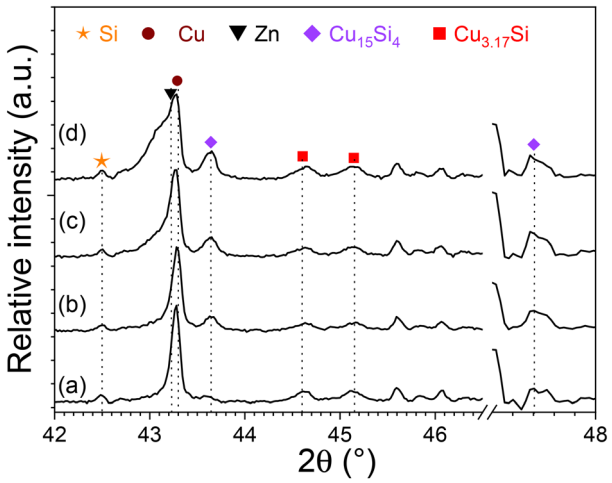

Fig. 6 XRD diffractograms between 42–51° of the contact mass PM-Zn0.30 recorded after reaction at (a) 1.5%, (d) 6.4%, (e) 10.2% and (f) 13.9% of Si conversion. The symbols indicate the peak positions of the Si, Cu, Zn, $Cu_{15}Si_4$, and $Cu_{3.17}Si$ crystalline phases, which were indexed with the PDF 27-1402, 04-0836, 04-0831, 14-4307 and 76-7859 patterns, respectively.

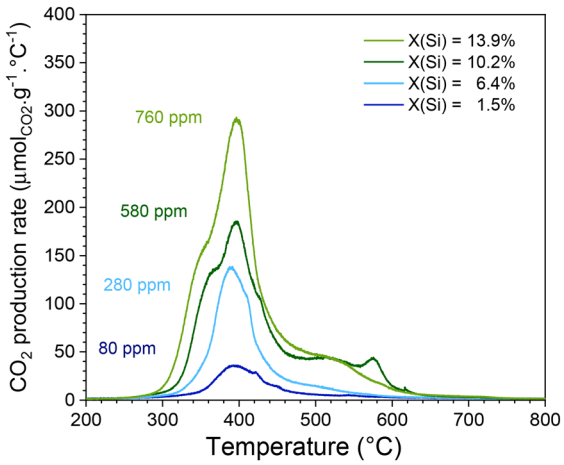

Fig. 5 TPO curves of the PM-Zn0.30 contact mass recorded after catalytic test at 1.5%, 6.4%, 10.2% and 13.9% of Si conversion.

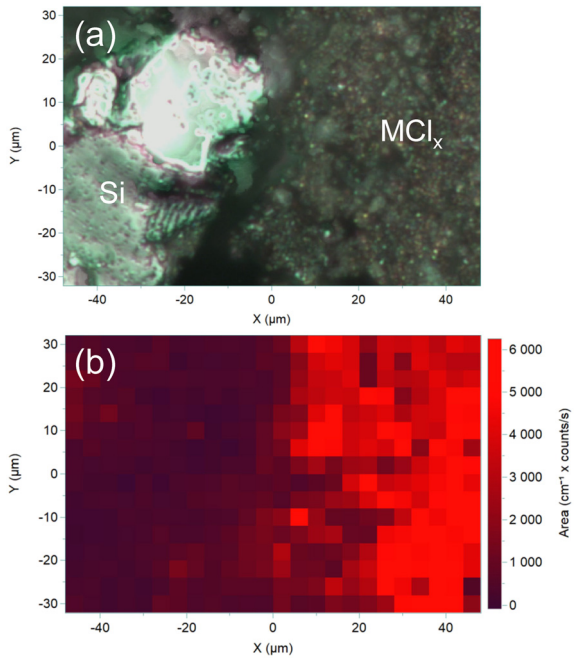

Fig. 7 (a) Optical image and (b) hyperspectral Raman image of the area between 1130 and 1736 cm^{-1} (disordered graphite bands) of contact mass PM-Zn0.30 after reaction at X(Si) = 1.5%. The fluorescence background was subtracted.

disordered graphite, due to resonance effects explaining its detection even at only 80 ppm of carbon.[42,43] Fig. 7b displays the hyperspectral Raman image of the intensity of disordered graphite, showing that it was localized on chloride particles supporting that CH_3Cl cracking may occur on CuCl particles.[7] Even if the direct synthesis is performed industrially in a fluidized bed reactor allowing efficient heat transfer, industrial reactors are not perfectly homogeneous and local hot spots can still occur leading to thermal cracking.[2] Conversely, colder zones can also exist, in which chlorinated species may condense and promote secondary cracking reactions. In that regard, this work highlights the need to limit the quantity of residual CuCl during the reaction.

The formation of the carbon species was evidenced by SEM/EDS analysis at higher Si conversion. Indeed, SEM image of the contact mass PM-Zn0.30 after reaction at X(Si) = 13.9% exhibited two distinct textures: Si particles of approximately 50–80 μm and agglomerates of smaller particles corresponding to a chloride (Fig. 8).

Copper was present on the facets and edges of Si particles and also within the chloride. Zn was either mixed with Cu in chloride particles or present as zinc chloride. Carbon was exclusively localized in the chloride regions in agreement with the Raman hyperspectral image obtained at lower Si conversion.

To further prove the correlation between the locations of chloride particles and carbonaceous species, Raman mapping was conducted on the same area as SEM/EDS analysis (Fig. S10) using a Nano-GPS system (see the Experimental methods). Then, an area of 60 × 100 μm^2 (optical image in Fig. 9a corresponding to the red rectangle in Fig. S10) was selected.

The hyperspectral image of the intensity of disordered graphite (Fig. 9b) revealed that it was localized everywhere and not preferentially in the chloride rich regions, contrary to the Raman mapping performed at 1.5% of Si conversion (Fig. 7b). This shows that even if carbon was concentrated on the chloride particles, a small amount (detected as disordered graphite by Raman spectroscopy) was spread on Si particles probably limiting their accessibility.

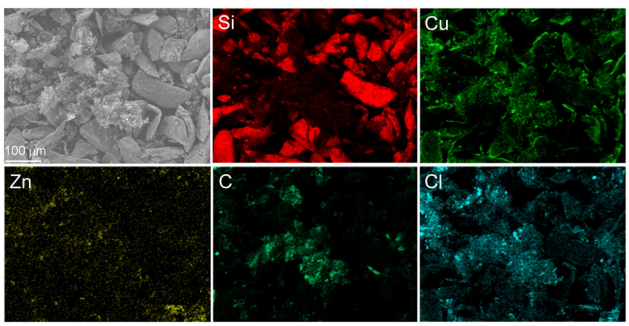

Fig. 8 SEM image of the contact mass PM-Zn0.30 after reaction at X(Si) = 13.9% and the corresponding EDS elemental mapping images.

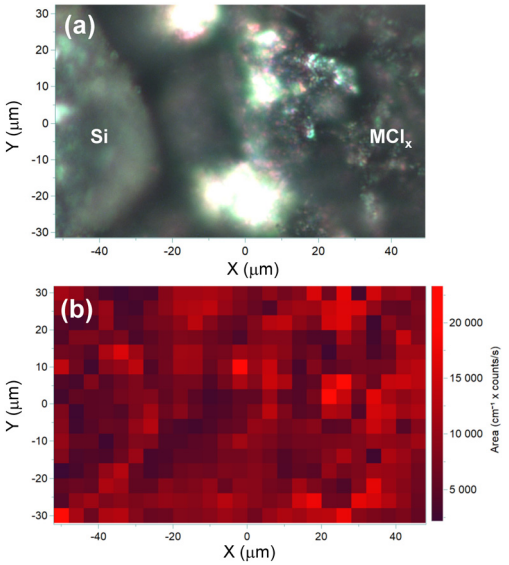

Fig. 9 (a) Optical image and (b) hyperspectral Raman image of the area between 1130 and 1736 cm^{-1} (bands of disordered graphite) of contact mass PM-Zn0.30 after reaction at X(Si) = 13.9%. The fluorescence background was subtracted.

4. Conclusions

Pretreatment at 310 °C of both non-promoted and promoted masses led to the formation of Cu_3Si as well as the undesired $Cu_{15}Si_4$ and Cu crystalline phases by the reaction between CuCl and Si. Furthermore, addition of Zn and $Cu_{0.9}Sn_{0.1}$ was shown to accelerate such reactions probably by formation of mixed chloride, which wets Si particles thereby favouring interfacial diffusion.

The addition of Zn and Sn was confirmed to improve the M2 formation rate at 295 °C. However, it also favours CH_3Cl cracking at the early beginning of the MCS synthesis and hence, coke formation. Even if the quantity of the Cu-rich phases was initially higher for the promoted masses, no significant differences were evidenced after reaction even at low Si conversion. In fact, coke containing disordered graphite, readily detected by Raman spectroscopy, was preferentially formed on the remaining chloride particles which act as a Cu reservoir. The presence of Zn and Sn within such particles could favour CH_3Cl cracking. By increasing the Si conversion, the quantity of coke increases linearly, associated with a spreading on Si particles probably limiting their accessibility. Therefore, the tangled positive and negative effects of Zn and Sn 'promoters' as well as the CuCl precursor highlight the need to carefully optimize their respective amounts in an industrial process.

Author contributions

L. Riviere: investigation, data curation, formal analysis, visualization, and writing – original draft. E. Blaser: supervision, resources, and methodology. M. Huet: supervision and resources. C. Rosier: funding acquisition,

project administration, and supervision. C. Geantet: supervision, resources, methodology, and validation. S. Loridant: funding acquisition, project administration, supervision, resources, methodology, validation, visualization, writing – review and editing.

Conflicts of interest

There are no conflicts to declare.

Data availability

The data supporting the findings of this study are available within the article and its supplementary information (SI). Supplementary information is available: thermodynamic calculations, scheme of catalytic testing apparatus, evolutions of temperature and relative pressure during pretreatment and reaction, XRD diffractograms, catalytic data, TPO curves, SEM images, optical image and Raman spectra. See DOI: https://doi.org/10.1039/d5cy01426c.

Acknowledgements

The ANRT association and the Elkem Silicones France company are acknowledged for the CIFRE grant of Lucie Riviere (2021-0925) and financial support, respectively.

References

1 The Socioeconomic Impact of the Silicones Industry in Europe, https://www.silicones.eu/wp-content/uploads/2018/09/ces_socio-economic_study_eu_final.pdf, (accessed 2025-10-03).
2 E. Blaser, C. Rosier, M. Huet, P. Chaurand, C. Geantet and S. Loridant, *Catal. Sci. Technol.*, 2021, **11**, 469–473.
3 Y. Zhang, J. Li, H. Liu, Y. Ji, Z. Zhong and F. Su, *ChemCatChem*, 2019, **11**, 2757–2779.
4 R. Voorhoeve, *Organosilanes: Precursor to silicones*, Elsevier, Amsterdam, 1967.
5 R. J. H. Voorhoeve, B. J. H. Geertsema and J. C. Vlugter, *J. Catal.*, 1965, **4**, 43–55.
6 R. A. Turetskaya, K. A. Andrianov, I. V. Trofimova and E. A. Chernyshev, *Russ. Chem. Rev.*, 1975, **44**, 212–226.
7 E. Blaser, C. Rosier, M. Huet, C. Geantet and S. Loridant, *Catal. Sci. Technol.*, 2022, **12**, 2006–2014.
8 L. Fredenucci-Caillod, *PhD thesis*, University of Lyon 1, 2006.
9 B. H. Kolster, J. C. Vlugter and R. J. H. Voorhoeve, *Recl. Trav. Chim. Pays-Bas*, 1964, **83**, 737–751.
10 G. Weber, D. Viale, H. Souha, B. Gillot and P. Barret, *Solid State Ionics*, 1989, **32**, 250–257.
11 J. Xu, S. Song, J. Li, Y. Ji, Z. Li, D. Fu, Z. Zhong, G. Xu and F. Su, *J. Catal.*, 2023, **419**, 99–111.
12 F. Zeng, Y. Zhu, B. Jin, Y. Ji, L. Shi, G. Xu, D. Fu, Z. Zhong and F. Su, *Appl. Catal., A*, 2022, **636**, 118582.
13 J. Xu, S. Song, Y. Zhu, B. Jin, Y. Ji, Z. Li, D. Fu, Z. Zhong, G. Xu and F. Su, *J. Catal.*, 2022, **410**, 280–293.
14 C. H. Bartholomew, *Appl. Catal., A*, 2001, **212**, 17–60.
15 T. J. Wessel and D. G. Rethwisch, *J. Catal.*, 1996, **161**, 861–866.
16 M. P. Clarke, *J. Organomet. Chem.*, 1989, **376**, 165–222.
17 W. J. Ward, A. Ritzer, K. M. Carroll and J. W. Flock, *J. Catal.*, 1986, **100**, 240–249.
18 J. P. Kim and D. G. Rethwisch, *J. Catal.*, 1992, **134**, 168–178.
19 K. M. Lewis, D. McLeod and B. Kanner, *Stud. Surf. Sci. Catal.*, 1988, **38**, 415–434.
20 C. Wang, T. Liu, Y. Huang, G. Wang and J. Wang, *Ind. Eng. Chem. Res.*, 2013, **52**, 5282–5286.
21 T. C. Frank, K. B. Kester and J. L. Falconer, *J. Catal.*, 1985, **95**, 396–405.
22 L. D. Gasper-Galvin, D. M. Sevenich, H. B. Friedrich and D. G. Rethwisch, *J. Catal.*, 1991, **128**, 468–478.
23 Y. Cui, Y. Zhu, B. Jin, K. Wang, J. Gao, L. Zhang, G. Xu, Z. Zhong and F. Su, *Ind. Eng. Chem. Res.*, 2024, **63**, 17778–17789.
24 Z. Ge, Y. Zhu, B. Jin, D. Zhao, J. Gao, L. Zhang, G. Xu, Z. Zhong and F. Su, *Appl. Catal., A*, 2024, **687**, 119941.
25 J. Geng, Y. Zhu, B. Jin, J. Gao, Z. Zhang, Z. Zhong, G. Xu and F. Su, *J. Catal.*, 2024, **429**, 115262.
26 H. Zhang, B. Jin, Y. Zhu, L. Ban, K. Wang, J. Xu, J. Gao, Z. Zhong, G. Xu and F. Su, *J. Catal.*, 2023, **425**, 143–154.
27 M. Mahmoodinia, H. Farooq, T. Røe, I.-H. Svenum and H. J. Venvik, *Ind. Eng. Chem. Res.*, 2023, **62**, 21579–21589.
28 Y. NuLi, B. Wang, J. Yang, X. Yuan and Z. Ma, *J. Power Sources*, 2006, **153**, 371–374.
29 C. Antunes Corrêa, M. Poupon, J. Kopeček, R. Král, P. Zemenová, J. Lecourt, N. Barrier, P. Brázda, M. Klementová and L. Palatinus, *Intermetallics*, 2017, **91**, 129–139.
30 R. R. Chromik, W. K. Neils and E. J. Cotts, *J. Appl. Phys.*, 1999, **86**, 4273–4281.
31 D. Lüdecke, *CALPHAD: Comput. Coupling Phase Diagrams Thermochem.*, 1987, **11**, 135–142.
32 M. E. Schlesinger, *Chem. Rev.*, 1990, **90**, 607–628.
33 H. Viitala, P. Taskinen and D. Lindberg, *CALPHAD: Comput. Coupling Phase Diagrams Thermochem.*, 2019, **67**, 101667.
34 R. Harry Morten, *PhD thesis*, Norwegian University of Science and Technology, 1992.
35 T. Glasson, *PhD thesis*, University of Lyon 1, 1999.
36 J. P. Agarwala and J. L. Falconer, *Int. J. Chem. Kinet.*, 1987, **19**, 519–537.
37 A. Le Valant, C. Comminges, C. Tisseraud, C. Canaff, L. Pinard and Y. Pouilloux, *J. Catal.*, 2015, **324**, 41–49.
38 B. Bolle, *PhD thesis*, University of Metz, 1994.
39 M. Mahmoodinia, H. Farooq, T. Røe, I.-H. Svenum and H. J. Venvik, *Ind. Eng. Chem. Res.*, 2023, **62**, 21579–21589.
40 K. Uchinokura, T. Sekine and E. Matsuura, *Solid State Commun.*, 1972, **11**, 47–49.
41 A. C. Ferrari and J. Robertson, *Phys. Rev. B: Condens. Matter Mater. Phys.*, 2000, **61**, 14095–14107.
42 A. C. Ferrari, *Solid State Commun.*, 2007, **143**, 47–57.
43 M. J. Madito, *Vib. Spectrosc.*, 2025, **139**, 103814.

